ChemComm

COMMUNICATION

View Article Online
View Journal

Cite this: DOI: 10.1039/d6cc02237e

Received 12th April 2026,
Accepted 14th May 2026

DOI: 10.1039/d6cc02237e

rsc.li/chemcomm

Design of a flexible aromatic gate to immobilize C_{60} in a ferritin cage

Taiga Suzuki,[a] Yuki Hishikawa,[a] Basudev Maity,[a] Yumie Nishiyama,[b] Kazunori Motai,[b] Yuhei Hayamizu,[b] Satoshi Abe[c] and Takafumi Ueno *[ad]

We report a crystal structure of a ferritin cage immobilizing pristine fullerene (C_{60}). Mutational studies and molecular dynamics (MD) simulations reveal that a flexible aromatic gate system is effective for C_{60} immobilization.

Structural stability and symmetry are key properties that facilitate design and engineering of protein assemblies. Protein cages are generally suitable templates that can leverage these properties, including DNA-binding proteins from starved cells (Dps),[1] ferritin,[2] small heat-shock proteins (HSP),[3] lumazine synthase (LS),[4] and encapsulin (Enc).[5] Ferritin is one of the most extensively studied protein cages. Ferritin cages exhibit high stability, retaining their cage structures at temperatures above 80 °C,[6–8] across a wide range of pH (pH 2–10.5),[6,9] in various denaturants,[10] and even in 50% organic solvents.[10,11] Typical ferritins assemble into a 24-mer cage with 2-, 3-, and 4-fold symmetry (Fig. 1).[12,13] Among these interfaces, the 2-fold symmetric interface is the most stable due to strong intersubunit interactions,[10,12] which enables the introduction of multiple mutations at this interface (Fig. 1).[8,14–17]

These properties of ferritins allow the immobilization of a broader range of molecules. The high tolerance for and efficiency of mutations in ferritins enable the rational design of diverse immobilization sites. Their compatibility with harsh environments including heat and organic solvents allows molecular complexation under such conditions,[15,18–20] thereby expanding immobilization targets to hydrophobic molecules. Despite this potential of ferritins, molecular immobilization in ferritins has been reported only for a limited range of molecules, including metal complexes,[20–22] small-molecule drugs,[23–25] and aromatic fluorescent dyes.[15] Beyond the reported targets, ferritins may also enable the immobilization of more challenging molecules, such as pristine fullerene (C_{60}). C_{60} is particularly difficult to immobilize in proteins because of its water insolubility and bulky spherical shape (diameter of 7 Å).[26] Although crystal structures of proteins complexed with a solubility-enhanced carboxylated fullerene derivative have been reported, crystal structures of proteins that immobilize C_{60} have not been reported.[27,28]

In this study, we report immobilization of C_{60} within a ferritin cage through molecular design. We designed a C_{60} immobilization site within the ferritin cage consisting of a near-spherical hydrophobic cavity and a phenylalanine gate (Phe gate) (Fig. 2a). The X-ray crystallography and UV–vis spectroscopy confirmed that C_{60} is localized at the designed immobilization site. Mutational studies and molecular dynamics (MD) simulations revealed that the flexibility of the Phe gate is essential for C_{60} immobilization. The findings provide design guidelines for engineering proteins that immobilize fullerenes *via* non-covalent interactions.

We designed a C_{60} immobilization site consisting of a near-spherical hydrophobic cavity and a Phe gate by glycine and phenylalanine substitutions, respectively (Fig. 2a). As a suitable template, we selected the 2-fold symmetric interface of recombinant horse spleen L-chain ferritin (Fr) without iron (apo-Fr), which is widely used and exhibits high structural stability

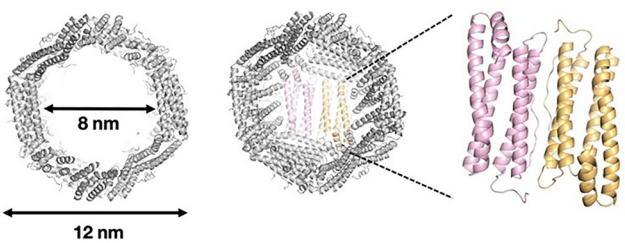

Fig. 1 The 24-mer cage structure of a ferritin protein and its 2-fold symmetric interface (PDB: 1DAT).

[a] School of Life Science and Technology, Institute of Science Tokyo, Nagatsuta-cho 4259, Midori-ku, Yokohama 226-8501, Japan. E-mail: ueno.t.bb33@m.isct.ac.jp
[b] School of Material Science and Technology, Institute of Science Tokyo, 2-12-1, Ookayama, Meguro-ku, Tokyo 152-8550, Japan
[c] School of Life and Environmental Sciences, Kyoto Prefectural University, 1-5 Hangi-cho, Shimogamo, Sakyo-ku, Kyoto 606-8522, Japan
[d] Research Center for Autonomous Systems Materialogy (ASMat), Institute of Integrated Research, Institute of Science Tokyo, Nagatsuta-cho 4259, Midori-ku, Yokohama 226-8501, Japan

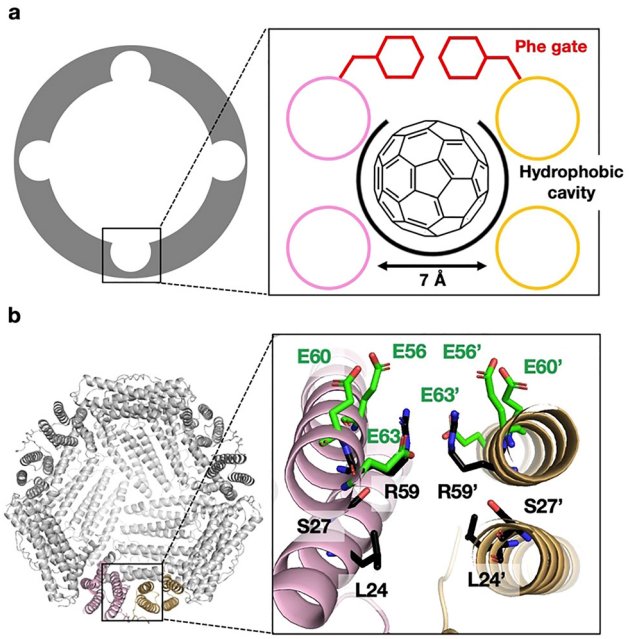

Fig. 2 (a) Schematic representation showing the near-spherical cavities with Phe gate at the interior wall of a ferritin cage for C_{60} immobilization. (b) The 2-fold symmetric interface of apo-Fr-WT (PDB: 1DAT). Selected residues for Phe and Gly mutations are shown as green and black sticks, respectively.

among ferritin cages.[6,12] Using this as a template, we previously introduced phenylalanine mutations to immobilize aromatic fluorescent dyes *via* π–π stacking.[8,15] While aromatic fluorescent dyes are generally planar, C_{60} is a bulky spherical molecule, which requires a different design for immobilization. For efficient uptake and immobilization of C_{60}, substitution with multiple aromatic amino acids[29] and a hemispherical hydrophobic cavity[27] have been suggested to be effective. Therefore, we designed a Fr mutant **apo-Fr-F3G3** (Fr-L24G/S27G/E56F/R59G/E60F/E63F). We replaced L24, S27, and R59 with Gly to create a cavity capable of accommodating C_{60} (Fig. 2b). In addition, E56, E60, and E63 at the cavity entrance were replaced with Phe to form a gate (Fig. 2b). **Apo-Fr-F3G3** was expressed and purified according to a reported method.[30] The 24-mer cage assembly of **apo-Fr-F3G3** was verified by Native PAGE, and the detailed cage structure was confirmed by X-ray crystallography.

Complex formation of C_{60} with **apo-Fr-F3G3** was performed in a mixed solvent consisting of 50% (v/v) methanol, 5% (v/v) PEG400, and 45% (v/v) buffer (50 mM Tris-HCl, 150 mM NaCl, pH 8.0 in the stock solution). The concentration of **apo-Fr-F3G3** in the reaction mixture was 10 μM, and C_{60} was added in excess. The reaction mixture was sonicated for 1 h, followed by heating at 70 °C for 24 h. The reaction mixture was then subjected to dialysis against the buffer (50 mM Tris-HCl, 150 mM NaCl, pH 8.0), followed by filtration (see supporting information). The resulting complex of **apo-Fr-F3G3** with C_{60} was named **C_{60}·Fr-F3G3** (Fig. 3a). Native PAGE confirmed that **C_{60}·Fr-F3G3** maintained the 24-mer cage assembly (Fig. 3b). The UV–vis spectrum of **C_{60}·Fr-F3G3** exhibited distinct absorption peaks at

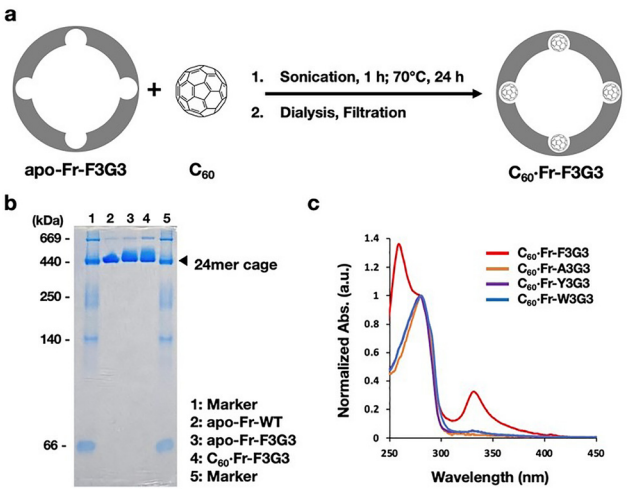

Fig. 3 Preparation of the C_{60}·Fr complex and selected characterization data. (a) Schematic representation of the synthetic procedure for **C_{60}·Fr-F3G3**. (b) Native PAGE analysis of **Fr-F3G3** before and after C_{60} complexation. (c) UV-vis absorption spectra of various ferritin mutants complexed with C_{60} (**C_{60}·Fr-X3G3**; X = F, Y, W, A) in aqueous buffer.

259 and 332 nm assigned to C_{60} (Fig. 3c).[31,32] Based on the absorbance of C_{60} at 332 nm and the protein concentration determined by the bicinchoninic acid (BCA) assay, 2.7 ± 0.1 C_{60} molecules per Fr cage were estimated, while 12 equivalent immobilization sites were designed per cage. The incomplete incorporation of C_{60} is likely due to restricted access of the C_{60} molecules through the channels of the Fr cage. This kinetic bottleneck may still persist due to the bulkiness of C_{60}, even under the harsh condition that expands the channels.[19,20] We also tested immobilization of C_{70} and buckyferrocene using the same procedure. However, UV-vis spectra did not indicate the immobilization of these fullerene species, likely due to the size and shape complementarity of the hydrophobic cavity (Fig. S4). We also explored C_{60} complexation with other mutants in which Phe was replaced with Tyr, Trp, or Ala (**apo-Fr-X3G3**; X = Y, W, A), but negligible absorption peaks from C_{60} were observed (Fig. 3c). These results indicate that the designed cavity selectively complexes C_{60}, and that the Phe residues are essential for this process.

To obtain structural evidence of C_{60} immobilization, we crystallized both **apo-Fr-F3G3** and **C_{60}·Fr-F3G3** and determined the X-ray structures at resolutions of 1.57 Å and 1.99 Å, respectively (Fig. 4 and Table S1 for crystallographic statistics). The structure of **apo-Fr-F3G3** showed formation of the near-spherical cavity (Fig. 4a). Both the $2F_o - F_c$ map in **C_{60}·Fr-F3G3** and the F_o(**C_{60}·Fr-F3G3**) − F_o(**apo-Fr-F3G3**) difference map showed a hollow quasi-spherical electron density located in the cavity (Fig. S6 and S7). The electron density was modeled as a C_{60} molecule. Refinement yielded a partial occupancy of C_{60} (0.5 per Fr dimer) which means a total of six C_{60} molecules out of 12 cavities were incorporated into the 24-mer cage. Both crystal structure and BCA/absorbance analysis suggest that the designed cavities were not fully but partially filled with C_{60} molecules.

The localization of C_{60} in the cavity of **C_{60}·Fr-F3G3** was further confirmed using the environmental dependence of

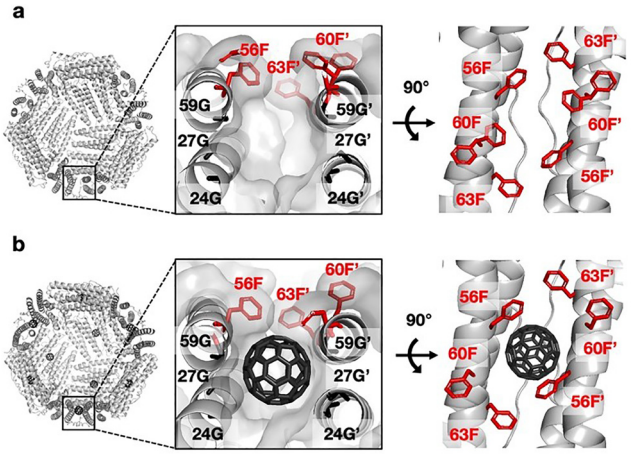

Fig. 4 Crystal structures showing the 24-mer cage of (a) **apo-Fr-F3G3** and (b) **C_{60}·Fr-F3G3**. The insets show the C_{60} binding site in apo form and C_{60} immobilized form. The modelled C_{60} molecule in **C_{60}·Fr-F3G3** is shown based on the electron density maps presented in Fig. S6.

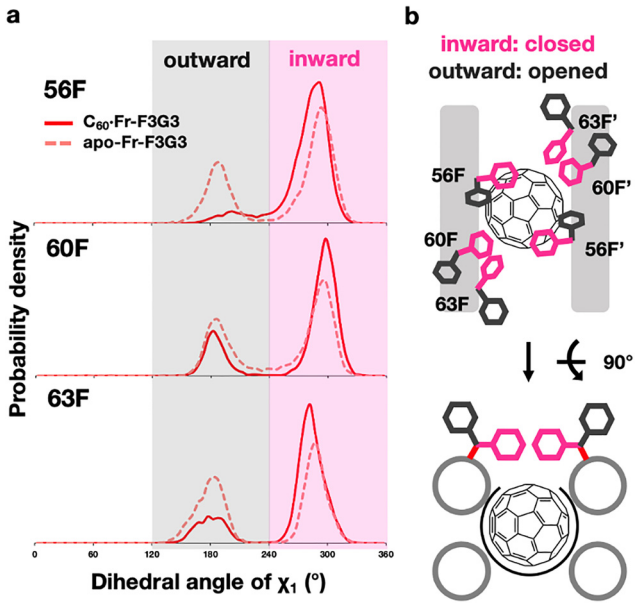

Fig. 5 Dynamic behaviour of the Phe gate analysed by MD simulations. (a) Distributions of χ_1 dihedral angles of Phe residues during 100 ns MD simulations of **C_{60}·Fr-F3G3** and **apo-Fr-F3G3**. (b) Representative conformations illustrating outward- and inward-oriented Phe residues at the two-fold symmetric interface relative to the immobilization site. The grey blocks represent B-helices from two subunits at the 2-fold symmetric interface.

the UV-vis spectra of C_{60}.[32–35] The cavity is formed by residues 24G, 27G, Y28, L31, A55, 59G, and L81, providing a hydrophobic environment (Fig. S8a). In the crystal structure of **C_{60}·Fr-F3G3**, the C_{60} molecule is located 3.1–4.0 Å from the nearest carbon atoms of these residues, consistent with hydrophobic interactions (Table S2).[36,37] In agreement with this, the absorption maxima (259 nm and 332 nm) suggest that C_{60} is located in a hydrophobic environment similar to chloroform (Fig. S9). The absence of any shoulder peak around 450 nm excludes the possibility of C_{60} aggregation (Table S3).[32,35] If C_{60} were located outside the cavity, it would be exposed to a more hydrophilic environment and form aggregates with other C_{60} molecules. The lack of such features supports localization of C_{60} within the hydrophobic cavity.

In addition to the hydrophobic cavity, the Phe residues also contribute to providing the hydrophobic environment and the isolation of C_{60}. In the crystal structure of **C_{60}·Fr-F3G3**, the C_{60} molecule is located 5.3–5.4 Å from the aromatic rings of 56F and 56F′, suggesting aromatic interactions (Fig. S8b).[38] To verify the interaction between Phe and C_{60}, MD simulations of **apo-Fr-F3G3** and **C_{60}·Fr-F3G3** were performed for 100 ns using the crystal structures as initial coordinates (Movie S1 and S2). To identify the conformation of Phe residues (56F, 60F, and 63F), χ_1 (N–Cα–Cβ–Cγ) dihedral angles were analysed, where 120–240° corresponds to outward orientations from the immobilization site and 240–360° corresponds to inward orientations (Fig. 5). Phe residues in **C_{60}·Fr-F3G3** frequently adopt inward orientations, whereas those in **apo-Fr-F3G3** exhibit flexible behaviour with both orientations (Fig. 5a). This increased probability of inward orientations suggests aromatic interactions between the Phe residues and C_{60}, which make the Phe side chains cover C_{60} at the cavity entrance (Fig. S10a). Therefore, the Phe residues act as a gate that dynamically opens and closes in the absence of C_{60}, and closes upon C_{60} immobilization.

To clarify the role of Phe in C_{60} immobilization, we compared **Fr-F3G3** and **Fr-A3G3**, focusing on two processes: uptake into the cavity and retention within the cavity. Experimentally, **Fr-A3G3** does not immobilize C_{60}, unlike **Fr-F3G3** (Fig. 3c). For the retention process, we performed an MD simulation using an *in silico*–generated model of **C_{60}·Fr-A3G3**, in which the aromatic rings were deleted from the crystal structure of **C_{60}·Fr-F3G3**. Surprisingly, C_{60} was consistently retained within the immobilization site in **C_{60}·Fr-A3G3** as in **C_{60}·Fr-F3G3** (Movie S3). Therefore, C_{60} retention within the immobilization site is considered to be primarily mediated by hydrophobic interactions within the cavity, whereas the Phe residues do not appear to be essential for retention. MM/GBSA analysis also supports this interpretation, suggesting that the hydrophobic cavity accounts for most of the binding energy and is sufficient for C_{60} immobilization (Fig. S11 and Table S4).[27] For the uptake process, we performed MD simulations using the crystal structures of **apo-Fr-F3G3** and **apo-Fr-A3G3**, with C_{60} placed inside the cage but outside the immobilization site (**apo-Fr-F3G3 + C_{60}** and **apo-Fr-A3G3 + C_{60}**) (Fig. 4a and Fig. S12, S13). C_{60} was attracted toward the vicinity of the immobilization site in **apo-Fr-F3G3 + C_{60}**, whereas C_{60} was dispersed in **apo-Fr-A3G3 + C_{60}** (Movie S4, S5 and Fig. S14). Therefore, Phe residues primarily contribute to the uptake of C_{60}, whereas the hydrophobic cavity governs the retention of C_{60} within the immobilization site.

To clarify the factors leading to C_{60} immobilization, we compared the behaviours of Phe, Tyr, and Trp gates. Experimentally, C_{60} immobilization was achieved only with the Phe gate and was not observed for the Tyr or Trp gates. This behaviour does not match the reported order of binding energies between C_{60} and aromatic amino acids (Trp > Tyr > Phe).[39–41] We also compared

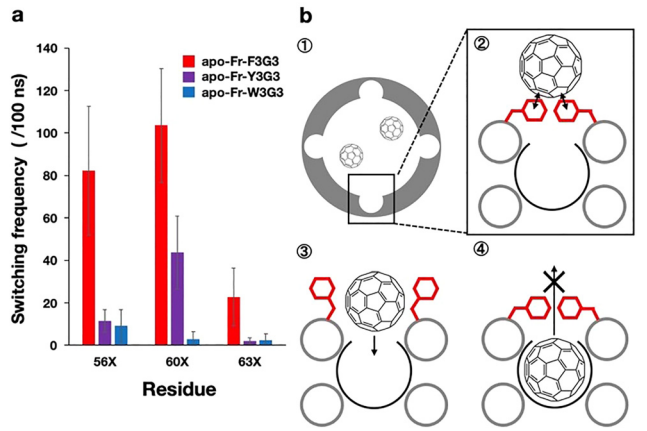

Fig. 6 (a) Frequencies of χ_1 dihedral-angle switching between inward- and outward-oriented states for residues 56X, 60X, and 63X during MD simulations of **apo-Fr-X3G3** (X = F, Y, W), reflecting differences in flexibility among Phe, Tyr, and Trp gates. (b) Proposed mechanisms of C_{60} immobilization by the Phe gate.

the flexibility of Phe, Tyr, and Trp residues in MD simulations of **apo-Fr-X3G3** (X = F, Y, W; Movie S2, S6, and S7). The flexibility was evaluated using the switching frequency of aromatic side chains between inward- and outward-oriented states, which correlated with the C_{60} immobilization trend (Fig. 6a). Tyr residues frequently adopt outward orientations through hydrogen bonding with Arg52 and Arg64, resulting in a dispersed arrangement of aromatic rings that weakens their ability to attract C_{60} (Fig. S15 and S16). Regarding Trp, steric crowding caused by the bulkiness of the indole ring and inter-residue aromatic interactions restricts side-chain reorientation, limiting gate opening and C_{60} access to the immobilization site (Fig. S17). In contrast, Phe residues can orient inward to form a closely positioned arrangement that attracts C_{60} through multipoint aromatic interactions, and flexibly reorient to open the gate, allowing C_{60} to enter the cavity (Fig. 6b, Fig. S14 and Movie S4).

In summary, we successfully immobilized C_{60} in a Fr cage by rationally designing a near-spherical hydrophobic cavity with a Phe gate. The immobilization of C_{60} in the cavity was confirmed by X-ray crystallography. We elucidated that the Phe gate facilitates immobilization of C_{60} through aromatic interactions and flexible opening and closing. This system contrasts with conventional static π-surface-based C_{60} host systems,[42–45] which are difficult to realize in proteins.[46] This work provides a new and feasible design strategy for immobilizing C_{60}. We are continuing to engineer the Fr cage, which could provide insights into factors affecting immobilization efficiency. This approach may be extended to incorporate hydrophobic molecules into proteins for applications in drug delivery and biohybrid materials.

Author contributions

The manuscript was written by T. S., B. M., S. A., and T. U., T. S., Y. Hi., Y. N., and K. M. performed experiments with the assistance of Y. Ha. T. S., Y. Hi., and B. M. solved and refined the crystal structures. T. S. performed molecular dynamics simulations and analyzed the trajectories. T. U. supervised the project.

Conflicts of interest

The authors declare no conflict of interest.

Data availability

All the data supporting the findings of the work are presented within the main text or supplementary information (SI). Supplementary information is available. See DOI: https://doi.org/10.1039/d6cc02237e.

Raw data can be obtained from the authors upon reasonable request. The atomic coordinates of the crystal structures have been deposited in the Protein Data Bank with the accession codes 21LO (C_{60}·Fr-F3G3), 21LP (apo-Fr-F3G3), 21LQ (apo-Fr-Y3G3), 21LR (apoFr-W3G3), 21LS (apo-Fr-A3G3).

Acknowledgements

This work was supported by JSPS KAKENHI Grant No. JP25H02254 to T. U. The authors thank the Facility Station Division and the Materials Analysis Division of the Research Infrastructure Management Center, Institute of Science Tokyo, for X-ray crystallographic analysis and MALDI-TOF-MS measurements, as well as the Integrative Bioscience Facility, Bioscience Center, Institute of Science Tokyo, for DNA sequence analysis. MD simulations were carried out using the TSUBAME 3.0 and 4.0 supercomputer at the Institute of Science Tokyo. The authors also thank Yutaka Matsuo for kindly providing buckyferrocene. ChatGPT (OpenAI) was used solely for language refinement.

References

1 R. A. Grant, D. J. Filman, S. E. Finkel, R. Kolter and J. M. Hogle, *Nat. Struct. Mol. Biol.*, 1998, **5**, 294–303.
2 D. M. Lawson, P. J. Artymiuk, S. J. Yewdall, J. M. A. Smith, J. C. Livingstone, A. Treffry, A. Luzzago, S. Levi, P. Arosio, G. Cesareni, C. D. Thomas, W. V. Shaw and P. M. Harrison, *Nature*, 1991, **349**, 541–544.
3 K. K. Kim, R. Kim and S.-H. Kim, *Nature*, 1998, **394**, 595–599.
4 K. Ritsert, R. Huber, D. Turk, R. Ladenstein, K. Schmidt-Bäse and A. Bacher, *J. Mol. Biol.*, 1995, **253**, 151–167.
5 M. Sutter, D. Boehringer, S. Gutmann, S. Günther, D. Prangishvili, M. J. Loessner, K. O. Stetter, E. Weber-Ban and N. Ban, *Nat. Struct. Mol. Biol.*, 2008, **15**, 939–947.
6 S. Stefanini, S. Cavallo, C.-Q. Wang, P. Tataseo, P. Vecchini, A. Giartosio and E. Chiancone, *Arch. Biochem. Biophys.*, 1996, **325**, 58–64.
7 X. Liu, W. Jin and E. C. Theil, *Proc. Natl. Acad. Sci. U. S. A.*, 2003, **100**, 3653–3658.
8 Y. Hishikawa, H. Noya, S. Nagatoishi, T. Yoshidome, B. Maity, K. Tsumoto, S. Abe and T. Ueno, *Chem. – Eur. J.*, 2023, **29**, e202300488.
9 R. R. Crichton and C. F. A. Bryce, *Biochem. J.*, 1973, **133**, 289–299.
10 M. C. Linder, H. R. Kakavandi, P. Miller, P. L. Wirth and G. M. Nagel, *Arch. Biochem. Biophys.*, 1989, **269**, 485–496.

11 K. K. W. Wong, H. Cölfen, N. T. Whilton, T. Douglas and S. Mann, *J. Inorg. Biochem.*, 1999, **76**, 187–195.
12 B. Gallois, B. L. d'Estaintot, M.-A. Michaux, A. Dautant, T. Granier, G. Précigoux, J.-A. Soruco, F. Roland, O. Chavas-Alba, A. Herbas and R. R. Crichton, *JBIC, J. Biol. Inorg. Chem.*, 1997, **2**, 360–367.
13 P. D. Hempstead, S. J. Yewdall, A. R. Fernie, D. M. Lawson, P. J. Artymiuk, D. W. Rice, G. C. Ford and P. M. Harrison, *J. Mol. Biol.*, 1997, **268**, 424–448.
14 Y. Hishikawa, B. Maity, N. Ito, S. Abe, D. Lu and T. Ueno, *Chem. Lett.*, 2020, **49**, 840–844.
15 Y. Hishikawa, T. Suzuki, B. Maity, H. Noya, M. Yoshizawa, A. Asanuma, Y. Katagiri, S. Abe, S. Nagatoishi, K. Tsumoto and T. Ueno, *Adv. Sci.*, 2025, **12**, 2417030.
16 B. Maity, J. Tian, T. Furuta, S. Abe and T. Ueno, *Cryst. Growth Des.*, 2023, **23**, 7448–7458.
17 J. Tian, B. Maity, T. Furuta, T. Pan and T. Ueno, *Angew. Chem., Int. Ed.*, 2025, **64**, e202504608.
18 B. Jiang, X. Chen, G. Sun, X. Chen, Y. Yin, Y. Jin, Q. Mi, L. Ma, Y. Yang, X. Yan and K. Fan, *Nano Today*, 2020, **35**, 100948.
19 I. Inoue, M. Chiba, K. Ito, Y. Okamatsu, Y. Suga, Y. Kitahara, Y. Nakahara, Y. Endo, K. Takahashi, U. Tagami and N. Okamoto, *Nanoscale*, 2021, **13**, 1875–1883.
20 R. Lucignano and G. Ferraro, *Molecules*, 2024, **29**, 4045.
21 B. Maity, Y. Hishikawa, D. Lu and T. Ueno, *Polyhedron*, 2019, **172**, 104–111.
22 A. Mohanty, A. Parida, R. K. Raut and R. K. Behera, *ACS Bio Med. Chem. Au*, 2022, **2**, 258–281.
23 R. Liu, P. J. Loll and R. G. Eckenhoff, *FASEB J.*, 2005, **19**, 567–576.
24 L. S. Vedula, G. Brannigan, N. J. Economou, J. Xi, M. A. Hall, R. Liu, M. J. Rossi, W. P. Dailey, K. C. Grasty, M. L. Klein, R. G. Eckenhoff and P. J. Loll, *J. Biol. Chem.*, 2009, **284**, 24176–24184.
25 S. Oakley, L. S. Vedula, W. Bu, Q. C. Meng, J. Xi, R. Liu, R. G. Eckenhoff and P. J. Loll, *PLoS One*, 2012, **7**, e32070.
26 H. W. Kroto, J. R. Heath, S. C. O'Brien, R. F. Curl and R. E. Smalley, *Nature*, 1985, **318**, 162–163.
27 K.-H. Kim, D.-K. Ko, Y.-T. Kim, N. H. Kim, J. Paul, S.-Q. Zhang, C. B. Murray, R. Acharya, W. F. DeGrado, Y. H. Kim and G. Grigoryan, *Nat. Commun.*, 2016, **7**, 11429.
28 H. Benyamini, A. Shulman-Peleg, H. J. Wolfson, B. Belgorodsky, L. Fadeev and M. Gozin, *Bioconjugate Chem.*, 2006, **17**, 378–386.
29 M. Liutkus, A. López-Andarias, S. H. Mejías, J. López-Andarias, D. Gil-Carton, F. Feixas, S. Osuna, W. Matsuda, T. Sakurai, S. Seki, C. Atienza, N. Martín and A. L. Cortajarena, *Nanoscale*, 2020, **12**, 3614–3622.
30 K. Iwahori, K. Yoshizawa, M. Muraoka and I. Yamashita, *Inorg. Chem.*, 2005, **44**, 6393–6400.
31 H. Ajie, M. M. Alvarez, S. J. Anz, R. D. Beck, F. Diederich, K. Fostiropoulos, D. R. Huffman, W. Kraetschmer and Y. Rubin, *et al.*, *J. Phys. Chem.*, 1990, **94**, 8630–8633.
32 T. Andersson, G. Westman, O. Wennerström and M. Sundahl, *J. Chem. Soc., Perkin Trans. 2*, 1994, 1097–1101.
33 I. Renge, *J. Phys. Chem.*, 1995, **99**, 15955–15962.
34 T. Andersson, K. Nilsson, M. Sundahl, G. Westman and O. Wennerström, *J. Chem. Soc., Chem. Commun.*, 1992, 604–606.
35 X. Chang and P. J. Vikesland, *Environ. Sci. Technol.*, 2011, **45**, 9967–9974.
36 R. F. de Freitas and M. Schapira, *MedChemComm*, 2017, **8**, 1970–1981.
37 J. Mihel, M. Šikić, S. Tomić, B. Jeren and K. Vlahoviček, *BMC Struct. Biol.*, 2008, **8**, 21.
38 S. K. Burley and G. A. Petsko, *Science*, 1985, **229**, 23–28.
39 A. de Leon, A. F. Jalbout and V. A. Basiuk, *Chem. Phys. Lett.*, 2008, **452**, 306–314.
40 V. A. Basiuk and E. González-Luciano, *Fullerenes, Nanotubes Carbon Nanostructures*, 2016, **24**, 371–379.
41 T. D. Marforio, A. Calza, E. J. Mattioli, F. Zerbetto and M. Calvaresi, *Int. J. Mol. Sci.*, 2021, **22**, 11567.
42 T. Haino, M. Yanase and Y. Fukazawa, *Angew. Chem., Int. Ed. Engl.*, 1997, **36**, 259–260.
43 P. D. W. Boyd, M. C. Hodgson, C. E. F. Rickard, A. G. Oliver, L. Chaker, P. J. Brothers, R. D. Bolskar, F. S. Tham and C. A. Reed, *J. Am. Chem. Soc.*, 1999, **121**, 10487–10495.
44 E. M. Pérez, L. Sánchez, G. Fernández and N. Martín, *J. Am. Chem. Soc.*, 2006, **128**, 7172–7173.
45 A. Sygula, F. R. Fronczek, R. Sygula, P. W. Rabideau and M. M. Olmstead, *J. Am. Chem. Soc.*, 2007, **129**, 3842–3843.
46 F. Trozzi, T. D. Marforio, A. Bottoni, F. Zerbetto and M. Calvaresi, *Isr. J. Chem.*, 2017, **57**, 547–552.